thesis title

Pruthvi Mehta

2021

Contents

Chapter 1

Introduction

Chapter 2

The Super Kamiokande Detector

2.1 Event Reconstruction

2.1.1 Vertex Reconstruction

For low energy events (events up to 100MeV), Super-Kamiokande currently uses BONSAI (Branch Optimisation Navigating Successive Annealing Interactions) for event reconstruction. Vertex reconstruction for Super-Kamiokande has undergone changes and improvements depending on the phase of the experiment. For Phase I of Super-Kamiokande, vertex reconstruction depended on a lattice of test vertices with 4m spacing throughout the detector, with a specific measure of goodness for each test vertex: the test vertex with the highest measure of goodness would have around it a more finely spaced grid, and the process would be repeated. For Phase II of Super-Kamiokande due to the reduced number of PMTs, this approach was no longer as successful as it was in Phase I and as a result the reconstruction perfomance declined, and BONSAI was created as a replacement. Instead of using a fixed grid which was the case with SK-I and SK-II, BONSAI creates test vertices by selecting groups of four PMT hits and seeing where the timing residuals of the PMT hits would be most reduced. After these test vertices have been indentified, a maximum likelihood fit over all the PMT hits in the event is performed, shown in Equation 2.1.

$$\mathcal{L}(\vec{x}, t_0) = \sum_{i=1}^{N_{\text{hit}}} \log(P(t - t_{\text{tof}} - t_0)) \tag{2.1}$$

where $(\vec{x}, t_0)$ is the test vertex, and $(P(t - t_{\text{tof}} - t_0))$ is the probablility density function of the timing residual, which for each PMT hit is defined as $(t - t_{\text{tof}} - t_0)$, where t_0 is the time of the interaction, t_{tof} is the time of flight from the interaction vertex position to the position of the hit PMT, t is the PMT hit time. The vertex resolution
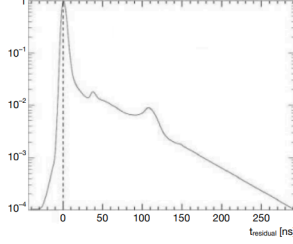
3

Figure 2.1: Probability density of the timing residual $P(t - t_{\text{tof}} - t_0)$, where t_0 use for the vertex reconstruction maximum likelihood fit. The peaks at 30ns and 100ns are caused by PMT after-pulsing. Figure from [?, nakanopdf]
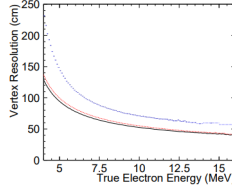

Figure 2.2: The vertex resolution (the point at which 68% of the events in the distance distribution between the actual and reconstructed vertex are contained) for the different SK phases. SK-I (Blue), SK-III (Red), SK-IV (Black). Figure from [?, nakanopdf]

2.1.2 Direction Reconstruction

Cherenkov light is emitted in a conical formation as electrons and positrons travel through water, with a Cherenkov angle of $\approx 42°$. BONSAI can reconstruct the direction of these particles by using this information along with the reconstructed vertex. This reconstruction occurs using a maximum likelihood function defined in Equation 2.2.

$$\mathcal{L}(\vec{d}) = \sum_i^{N_{20}} \log(f(\cos\theta_i, E)) \times \frac{\cos\theta_i}{a(\theta_i)} \qquad (2.2)$$

$f(\cos\theta_i, E)$ is the expected distribution of the angle between the vector of the direction $\vec{d}$ of the particle, and the observed Cherenkov photon from the position of the reconstructed vertex. The reason there is a spread in this energy distribution is because while the highest value of this distribution occurs at the cosine of the opening Cherenkov angle of $42°$, due to the particle travelling through the water being Coulomb scattered multiple times, there is a variation in the angle because of the varying particle energy. N_{20} is the number of hits whose residual hit time is within 20ns of the time of the reconstructed event, which is used in order to reduce the amount dark noise and scattered photons contribute to the direction reconstruction calculation. The variable $a(\theta_i)$ is used in the second term in Equation 2.2, and it is linked to the angle of incidence

4

of the photon on the PMT $a(\theta_i)$, and is a correction factor stemming from the acceptance of PMTs and therefore linked to the shape of the PMT and it's acrylic case.

Chapter 3

Super-Kamiokande Detector Calibration

Chapter 4

The UK Light Injection System

Chapter 5

Super-Kamiokande Gadolinium Upgrade

Chapter 6

Measurement of Neutral Current Quasielastic Interactions with Super-Kamiokande Gadolinium Upgrade

6.1 Bonsai output reconstruction quantities

Due to this analysis looking specifically at the low energy region, a fitter specific to low energies (called LOWFIT) is used to reconstruct events.

Both MC and data neutrino events undergo a reconstruction phase, where the low-energy fitter BONSAI is applied to the event. This reconstruction is carried out using timing and cable information, however charge information is omitted. The ouput of BONSAI gives information which will be used in the reduction phase of the data and allow for the selection of the NCQE sample. BONSAI is a low-energy fitter used in the few-MeV to tens of MeV energy range, therefore suitable for this analysis. Its directional reconstruction uses the fitted vertex and maximises for direction while it's energy reconstruction of the event is based upon the number of hit PMTs. Equation 6.1 shows how the vertex reconstruction is formulated, where w_i is the Gaussian hit weight of the PMT, t_i is the hit time of the PMT and x_i is the position of the hit PMT.

$$g(\vec{v}) = \sum_{i=1}^{N} w_i e^{-0.5(t_i - |\vec{x_i} - \vec{v}|/c)/\sigma)^2} \tag{6.1}$$

The following quantities comprise the BONSAI output, the first two being help-ful spectator variables and the latter five constituting parameters which are used

in the reduction phase of the analysis, from which the neutrino NCQE sample is determined.

Neutrino vertex direction

This vector points towards the direction which is an average over all the Cherenkov cone axes which are produced, due to there being multiple leptons induced in the interaction.

Neutrino vertex position
The reconstructed location of the neutrino interaction event.
Reconstructed energy
In line with the standard SK low energy analysis definition, this energy is simply the reconstructed energy with the 0.511 MeV electron mass omitted. The range for Erec in this variable is 3.49 MeV to 29.49 MeV - the estimated kinetic energy under the hypothesis that the event is a singular electron.

Dwall
This variable gives the minimum distance of the neutrino vertex position from the closest wall of the Super-Kamiokande detector.

Effwall
Thus variable gives the distance between the neutrino vertex posiiton and the closest wall, but moving back from the vertex position along the neutrino vertex direction vector.

Vertex direction and goodness coefficient
The coefficient $ovaQ$ (defined in Equation 6.2) describes the quality of the vertex reconstruction. It consists of two parameters g_{vtx}^2 and g_{dir}^2 where the former describes the goodness of the vertex which is based on PMT hit timings, and increases the sharper an event is in time. The latter is the directional goodness and measures the azimuthal uniformity in the ring pattern produced by the Cherenkov cone, which decreases the more uniform an event is in space. As a result of this, $ovaQ$ increases the more uniform and sharp in time an event is.

$$\text{ova } Q = g_{\text{vtx}}^2 - g_{\text{dir}}^2 \tag{6.2}$$

g_{vtx} is calculated using a fit of the PMT timing distribution and using the hit times of the PMT it is defined asin Equation6.3.

$$g_{\text{vtx}} = \frac{\sum_i w_i e^{-\frac{1}{2}(\frac{\Delta t_i}{\sigma})^2}}{\sum_i w_i} \text{ with } w_i = -\frac{1}{2}(\frac{\Delta t_i}{\omega})^2 \tag{6.3}$$

Here $\sum_i w_i$ is the weight given to the i-th hit PMT for the reduction of dark noise, where ω has a value of 60ns. σ has a value of 5ns which is used to test the goodness, and as a result, a sharp timing distribution produces a large vertex goodness. g_{dir} is calculated by looking at how spatially uniform the hit PMTs

are around the reconstructed neutrino vertex direction. In order to quantify this uniformity, the Kolmogorov-Smirnov (KS) test is used as in Equation 6.4.

$$g_{\text{dir}} = \frac{\max_i\{\angle_{\text{uni}}(i) - \angle_{\text{data}}(i)\} - \min_i\{\angle_{\text{uni}}(i) - \angle_{\text{data}}(i)\}}{2\pi} \tag{6.4}$$

where $\angle_{\text{data}}(i)$ is the azimuthal angle of i-th hit real PMT included in the number of hits in 50ns. $\angle_{\text{uni}}(i) = 2\pi i/N_{50}$ is the azimuthal angle of the i-th virtual PMT hit, but only when uniform distribution of the hits is assumed. As the uniformity of the hit pattern increases, the goodness decreases.

Cherenkov angle $theta_C$

For relativistic electrons in water, the value of the Cherenkov opening angle is $\approx 41°$, due to the relation:

$$\cos\theta_{\text{Cherenkov}} = \frac{1}{n\beta} \tag{6.5}$$

where $\beta = v/c \approx 1$ and n is the refractive index of water, 1.33. However due to other particles in the simulation, such as protons or muons, the Cherenkov cone is expected to be narrower, or if multiple leptons are present, the Cherenkov cones will be less distinct and more spread out, leading to deviations from the 41°value.

6.1.1 True neutron tagging information

6.1.2 Primary selection criteria

6.1.3 Secondary selection criteria

When the neutron vertex is found by this method, 14 variables which describe different aspects of the neutron candidate are calculated. For each of the neutron candidates the vector of these variables are computed and fed into the neural network and this produces an output value which is between 0 and 1. These variables relate to different features regarding categorising hits from neutron capture on Gd or H, including the number of the hits from neutron capture, the isotropy of these hits, the Cherenkov angles of these hits and the position of the neutron vertex in the detector when capture occurs. A description of these variables are given as follows:

N10nvx

This is the number of hits in the 10ns sliding window of the neutron candidate

N300S

Excluding the number of hits in the 10ns sliding window (N10nvx), this is the number of hits in the extended window of 300ns.

NcS

This variable is defined as:

$$NcS = N10nvx - Nclushit \tag{6.6}$$

Where $Nclushit$ is the number of clusterised hits: if hit i and j are hits on PMTs, then for hit i and hit j the hit vector $\hat{r}_i$ can be written as:

$$\hat{r}_i = \frac{\overrightarrow{PMT_i} - \overrightarrow{VTX_n}}{\left\| \overrightarrow{PMT_i} - \overrightarrow{VTX_n} \right\|} \tag{6.7}$$

where the angle at the point of the neutron capture vertex between $\hat{r}_i$ and $\hat{r}_j$ of the PMT hits is defined as:

$$\theta_{ij} = \arccos\left(\hat{p}_i \cdot \hat{p}_j\right) \tag{6.8}$$

where the hits are defined as clustered if θ_{ij} is less than 14

llrca

This variable is the log likelihood ratio calculated using triplets of hits from N10nvx that make up a rudimentary Cherenkov cone, from which the opening angle θ is calculated. Two PDFs (θ_{Ci}) and (θ_{Ci}) are calculated from each θ_{Ci} where p_s and p_b are the probability density functions of θ_C depending on whether the hits come from a true neutron capture on Gd or H or a false neutron capture which makes up the background. The log likelihood ratio variable is computed using Equation 6.9.

$$llrca = \sum_{i \in \{triplets\}} \log\left(\frac{f_B\left(\theta_{Ci}\right)}{f_S\left(\theta_{Ci}\right)}\right) \tag{6.9}$$

beta-n

These variables (where n = 1,2,3,4,5) are defined using Legendre polynomials, shown in Equation 6.10, which gives the isotropy of the Cherenkov hits.

$$beta - n = \frac{2}{N10nvx(N10nvx - 1)} \sum_{i \neq j} Legendre_n\left(\cos\theta_{ij}\right) \tag{6.10}$$

where $Legendre_n$ gives the Legendre polynomial of order n and $theta_{ij}$ is the angle between hit PMTs relative to the neutron capture vertex.

ndwall

This parameter, similar to dwall, gives the shortest distance of the neutron capture vertex from the wall of the Super-Kamiokande tank.

ntowall

This variable (similar to effwall), gives the distance of the neutron capture vertex from the wall, however, unlike ndwall it gives the direction of the neutron capture specifically along the direction of the centre of the hits. The direction ($\overrightarrow{R}$) is given by:

$$\overrightarrow{\mathrm{dir}} = \sum_{i=1}^{N10nvx} \hat{p}_i \tag{6.11}$$

Chapter 7

Systematic and statistical uncertainty calculations

7.1 Systematic uncertainty calculation methodology

The systematic uncertainities for this analysis are calculated using the probablity distribution functions of each quantity appearing in the formula for the mean neutron multiplicity, which is given by:

$$M = \frac{\#n_{\text{det}} - R \times \#\nu_{\text{det}}}{T} \frac{1}{\#\nu_{\text{det}}} \tag{7.1}$$

By random sampling the probability distribution functions for each of the terms in Equation (7.1) one can calculate the multiplicity probability distribution functions for both the statistical uncertainty and the systematic uncertainty. The statistical uncertainty for the value for the multiplicity is related to the variation in the number of detected neutrons, while the systematic uncertainty is related to the variation on the tagging efficiency and the background rate. The total search time for the tagged neutrons is dependent on the number of "windows" in which the neutron is searched for in, and therefore the term for the number of detected neutrinos. Because any variation on the number of neutrinos which are detected is unrelated to the value for the mean neutron multiplicity, calculating a probability mass function for the number of neutrinos is uneccessary.

A Poissonian distribution is used to model the distribution for the number of detected neutrons, due to its value being approximated by counting the positives in the timing window that the neutron tagging search is carried out in. The mean value of this Poisson distribution is denoted in Equation (7.2).

$$PMF\left(\#n_{\text{det}}\right) = \frac{1}{(\#n_{\text{det}})!} \left\langle \#n_{\text{det}} \right\rangle^{\#n_{\text{det}}} e^{-\left\langle \#n_{\text{det}} \right\rangle} \tag{7.2}$$

Regarding the background rate, this is estimated from dummy spill data, but it's error is associated with the statistical variation of the Monte Carlo size that the backround rate is associated with, and secondly the change of the background rate value during the SK-V period. The statistical variation of the MC is modelled using a Gaussian, while the uncertainty relating to time variation is characterised by its own probability distribution function. In contrast, the tagging efficiency is model dependent and has systematic uncertainties relating to this. The two ways in which the systematic error are estimated are either using MC re-weighting or MC regeneration.

For the MC-reweighting approach, weights are applied to a quantity and the tagging efficiency of the re-weighted MC is extracted. The general methodology is to have the input of a model (given by a set of parameters) and to vary them one by one and then calculate the reweighted tagging efficiencies - the set of relative discrepancies δ_i are computed from this set of reweighted tagging efficiencies T_i and the nominal tagging efficiency T_{nom} using Equation (7.3).

$$\delta_i = \frac{T_i - T_{\text{nom}}}{T_{\text{nom}}} \quad i \in \{ \text{ parameters } \} \tag{7.3}$$

These relative discrepancies δ_i are used to calculate the one indivdual discrepancy $\delta_{reweighted}$ that would describe the final deviation from the nominal tagging efficiency T_{nom} due to the systematic error. $\delta_{reweighted}$ describes the model which has been produced through 1σ variations of these parameters, therefore the final probability distribution function which describes the deviation from the nominal MC has a Gaussian distribution with the standard deviation being equal to $\delta_{reweighted}$.

The other method to estimate the systematic error on the tagging efficiency is the method of Monte Carlo regeneration. This is carried out by varying a parameter then regenerating the whole Monte Carlo and then extracting the tagging efficiency - therefore unlike with MC re-weighting there is no set of discrepancies δ_i but instead two single discrepancies δ_{min} and δ_{max}. The resulting probability distribution which describes the deviation from the nominal Monte Carlo is a Gaussian which has the mean and standard deviation relating to the discrepancies shown in Equation (7.4).

$$\begin{cases} \mu = \frac{\delta_{\text{max}} + \delta_{\text{min}}}{2} \\ \sigma = \frac{\delta_{\text{max}} - \delta_{\text{min}}}{2} \end{cases} \tag{7.4}$$

7.2 Neutrino beam flux uncertainty

The uncertainty on neutrino beam fluxes can also be evaluated by looking at the dependence of the tagging efficiency on the flux variations. The beam fluxes

for the four flavour modes $(\nu_e \overline{\nu_e} \nu_\mu \overline{\nu_\mu})$ have the fractional uncertainties given for each mode, FHC and RHC. The binned uncertainties are shown in Figure .

Each individual bin for the flux is increased/decreased by its error, the Monte Carlo re-weighting method is then used to extract the taggging efficiency for each flux bin, and Equation (7.5) is used to calculate the fractional uncertainty.

$$\delta_i(\pm\sigma) = \frac{T_i(\pm\sigma) - T_{\text{nom}}}{T_{\text{nom}}} \quad i \in \{ \text{ each flux bin } \} \tag{7.5}$$

Figure 7.1 shows the fractional errors calculated from the reweighted Monte Carlo, with the red bars showing the -1σ variation and the blue bars showing the +1σ variation. Table **??** contains the value for the total fractional uncertainty resulting from the neutrino beam flux, which was calculated using Equation (7.6), where the maximum value between the increased and decreased discrepancy is taken and summed over to produce the final neutrino flux beam uncertainty value.

$$\delta_{\nu \text{ flux}} = \sum_{i\in\{ \text{ bins } \}} \max\left[|\delta_i(+\sigma)|, |\delta_i(-\sigma)|\right] \tag{7.6}$$
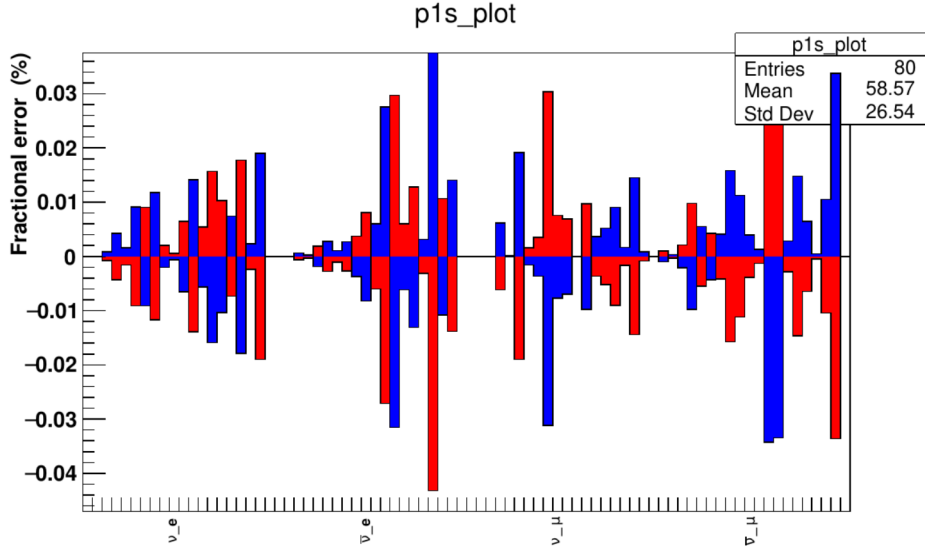

Figure 7.1: Tagging efficiency fractional uncertainties caused by neutrino beam flux discrepancies. From left to right the sections in this plot are comprised of the beam fluxes elements of $(\nu_e \overline{\nu_e} \nu_\mu \overline{\nu_\mu})$ respectively.

Parameter	Interaction	Type	Value
p_F^O	CCQE	^{16}O Fermi momentum	225 ± 31MeV/c
E_B^O	CCQE	^{16}O binding energy	27 ± 9MeV
M_A^{CCQE}	CCQE	Axial mass	1.2 ± 0.41GeV/c^2
$2p2h$			
C_{AS}^{RES}	2p2 h	Normalization par.	1.0 ± 1.0
M_A^{RES}	CC and NC1π	Axial form factor	1.01 ± 0.12
BG_A^{RES}	CC and NC1 π	Axial mass	0.95 ± 0.15GeV/c^2
CC other	CC and NC1π	I $= 1/2$ continuum background	1.3 ± 0.2
CC coherent	CC other	E-dependent par.	0.0 ± 0.4
NC other	CC coherent	Normalization par.	1.0 ± 0.3
NC coherent	NC other	NC-dependent par.	1.0 ± 0.3
		Normalization par.	1.0 ± 0.3
FSe^-Bremsstrahlung	CCν_e	Normalization par.	1.00 ± 0.03

Table 7.1: Neutrino cross section parameters

7.3 Neutrino cross section uncertainty

A group of default neutrino cross section values are used to make up the nominal Monte Carlo from which the tagging efficiency is calculated. The values of the parameters that determine the cross sections are shown in Table 7.1. Each of the parameter values relate to a specific interaction type and are either a normalisation parameter or a paramater which show a kinematic dependence. The Monte Carlo re-weighting method is used to reweight the nominal Monte Carlo on an event by event basis with each parameter value being increased and decreased by its uncertainty, and for each reweighted Monte Carlo the equivalent tagging efficiency value is extracted. Equation (7.7) shows how the fractional discrepancies are extracted from the nominal and reweighted tagging efficiency values.

$$\delta_i(\pm\sigma) = \frac{T_i(\pm\sigma) - T_{\mathrm{nom}}}{T_{\mathrm{nom}}} \quad i \in \{ \text{ parameters } \} \tag{7.7}$$

Figure 7.2 shows the reweighted Monte Carlo fractional uncertainty plotted for the FHC sample. Since this sample contains a lot of NCother interactions, the uncertainty for this interaction type is greater than for the others.

7.4 Pion final state interaction (FSI) and secondary interaction (SI) uncertainties

The neutrino-nucleus interaction simulator used in this analysis (NEUT) handles pion final state interactions and secondary interactions using a cascade
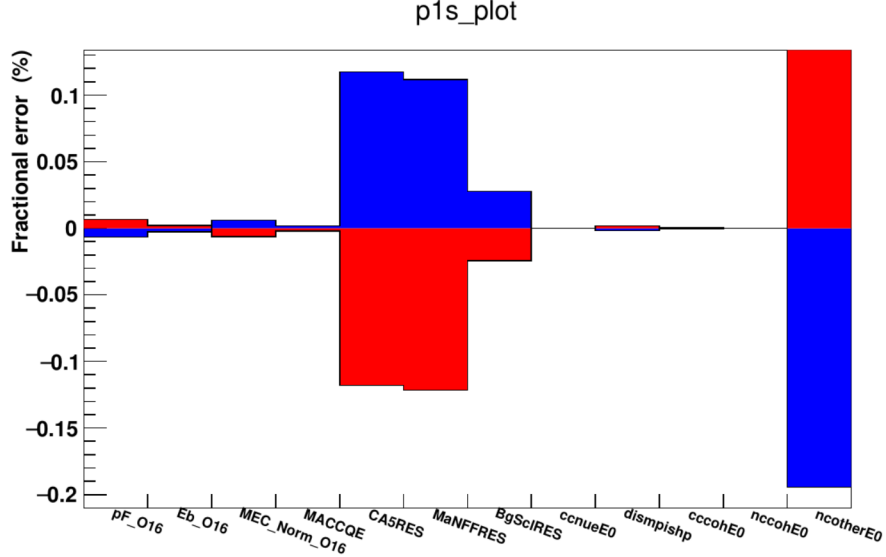
Figure 7.2: Tagging efficiency fractional uncertainty caused by the cross-section parameters variations for the FHC mode

model. This cascade model contains parameters which will have uncertainties on them and these will be tranferred to a possible change in the tagging efficiency.

Depending on the momentum of the pions, different interaction types occur in the model. For pions with a momentum less than 500 MeV, the interactions in place are absorption (ABS), quasi-elastic scattering (QE) and charge exchange (CX)./cite Absorption occurs when the incident pion is absorbed by the nucleus and no pions remain in the final state. Quasi-elastic (QE) scattering occurs when there is only one pion observed in the final state and it has the same charge as the incident beam. Charge exchange occurs when the charged pion interacts wtht he nucleus and a single π_0 can be seen in the final state.

For pions with a momentum of greater than 500 MeV, a different set of interactions are used. Inelastic interactions (INEL) can now produce hadrons and replace absorption processes, but quasi-elastic scattering (QEH) and charge exchange (CXH) will still occur. The final state interaction parameters and the pion momentum range they are used in can be seen in Table 7.2. Each parameter scales the relevant very small proability of the charged pion interaction at every stage of the intra-nuclear cascade, aside from the parameter for charge exchange which scales only the fraction of low momentum QE scattering.

A set of paramater variations which determine a surface in paramater space have been estimated by pion scattering experiments, the values for which are shown in Table 7.3. The 1σ surface has been explored using the nominal Monte Carlo re-weighting method and the analagous tagging efficiency uncertainty is

Parameter	Description	Momentum Region (MeV/c)
f_{ABS}	Absorption	< 500
f_{QE}	Quasi-elastic scatter	< 500
f_{CX}	Single charge exchange	< 500
f_{QEH}	Quasi-elastic scatter	> 500
f_{CXH}	Single charge exchange	> 500
f_{INEL}	Hadron (N + nπ) production	> 500

Table 7.2: Table showing the pion final state interaction parameters in NEUT and the pion momentum range they are used in

shown in Equation 7.8, and the uncertainty stemming from the models shown in Table 7.3 is shown in Figure 7.3

$$\delta_i = \frac{T_i - T_{\text{nom}}}{T_{\text{nom}}} \quad i \in \text{ parameter vector} \tag{7.8}$$
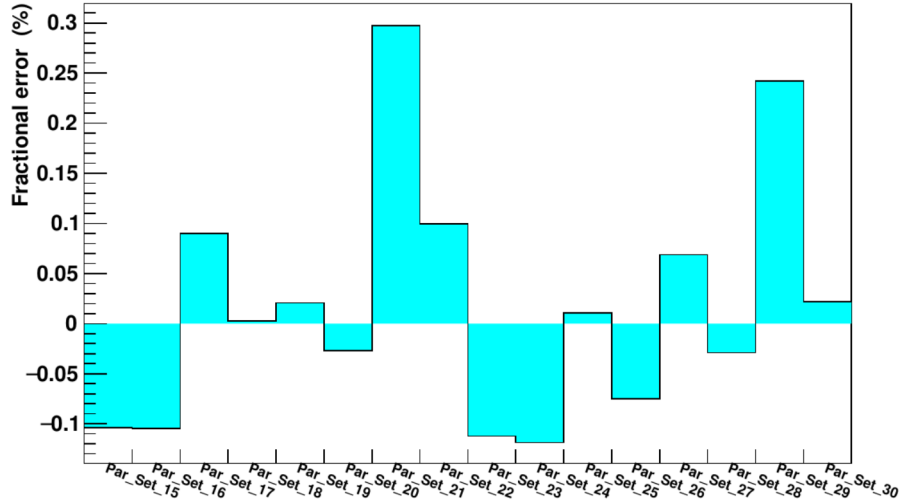

Figure 7.3: Tagging efficiency fractional uncertainty caused by the variation in the FSI/SI model parameters for the FHC mode.

7.5   Nucleon final state interactions

Uncertainties regarding the nucleon final state interactions can change the number of nucleons knocked out of ^{16}O, therefore how the tagging efficiency is changed due to the variation in nucleon final state interactions needs to be

Set	ABS	QE	CX	INEL	QEH	CXH
Nominal	1.1	1.0	1.0	1.0	1.8	1.8
	0.7	0.6	0.5	1.5	1.1	2.3
	0.7	0.6	1.6	1.5	1.1	2.3
Hadron production Up	1.6	0.7	0.4	1.5	1.1	2.3
	1.6	0.7	1.6	1.5	1.1	2.3
	0.6	1.4	0.6	1.5	1.1	2.3
	0.7	1.3	1.6	1.5	1.1	2.3
	1.5	1.5	0.4	1.5	1.1	2.3
	1.6	1.6	1.6	1.5	1.1	2.3
	0.7	0.6	0.5	0.5	2.3	1.3
	0.7	0.6	1.6	0.5	2.3	1.3
	1.6	0.7	0.4	0.5	2.3	1.3
Hadron production Down	1.6	0.7	1.6	0.5	2.3	1.3
	0.6	1.4	0.6	0.5	2.3	1.3
	0.7	1.3	1.6	0.5	2.3	1.3
	1.5	1.5	0.4	0.5	2.3	1.3
	1.6	1.6	1.6	0.5	2.3	1.3

Table 7.3: Pion FSI/SI model parameter nominal value and variations grouped according to inelastic hadron production value

Abbreviation	Description of uncertainty	Fractional uncertainty
x_{mfp}^N	Nucleon mean free path (total rescattering probability)	$\pm 20\%$
x_{cex}^N	Nucleon charge exchange probability	$\pm 50\%$
x_{el}^N	Nucleon elastic reaction probability	$\pm 30\%$
x_{inel}^N	Nucleon inelastic reaction probability	$\pm 40\%$
x_{abs}^N	Nucleon absorption probability	$\pm 20\%$
x_{π}^N	Nucleon π-production probability	$\pm 20\%$

Table 7.4: Nucleon final state interaction parameters of the hA model executed inside GENIE.

investigated. This uncertainty is extracted using GENIE, a Monte Carlo event generator which contains the INTRANUKE (hA) intranuclear transport model. The uncertainties in the in the total scattering probability for hadrons inside the target nuclei (x_{mfp}^N) and the uncertainties in the likelihood of each hadron rescattering method: (elastic (x_{el}^N), inelastic (x_{inel}^N), charge exchange (x_{cex}^N), pion production (x_{π}^N) and absorption (x_{abs}^N)) are taken into account. The fractional uncertainties for these modes for pions is shown in Table 7.4.

A nominal GENIE Monte Carlo sample is generated (different from the previously used NEUT Monte Carlo) and this shifted using the re-weighting method to a varied GENIE Monte Carlo by individually increasing and decreasing the parameters in Table 7.4 by its error. For each shifted Monte Carlo produced, the fractional uncertainty can be written as in Equation 7.9.

$$\delta_i(\pm\sigma) = \frac{T_i(\pm\sigma) - T_{\text{nom}}}{T_{\text{nom}}} \quad i \in \{ \text{ parameters } \} \tag{7.9}$$

The tagging efficiency fractional uncertainties are displayed in Figure 7.4, showing which parameter from Table 7.4 each uncertainty has arisen from.

7.6   Muon and pion capture on ^{16}O

Neutrons are produced from negative muon capture on ^{16}O as show in Equation 7.10.

$$\mu^{-16}\text{O} \longrightarrow \nu_\mu \text{n}^{15}\text{ N} \tag{7.10}$$

Direct neutrons are produced from pion capture on ^{16}O, but also a number of evaporation neutrons that leave the nucleus. For the capture of muons and pions on ^{16}O, the energy spectra of the neutrons produced have been measured: for muons the spectra can range up to 15MeV, while in the case of pions the spectra can reach up to 100MeV.

Geant4 simulates the capture processes for muons and pions, but there are alternate models that can be used: for example, the Chiral Invariant Phase
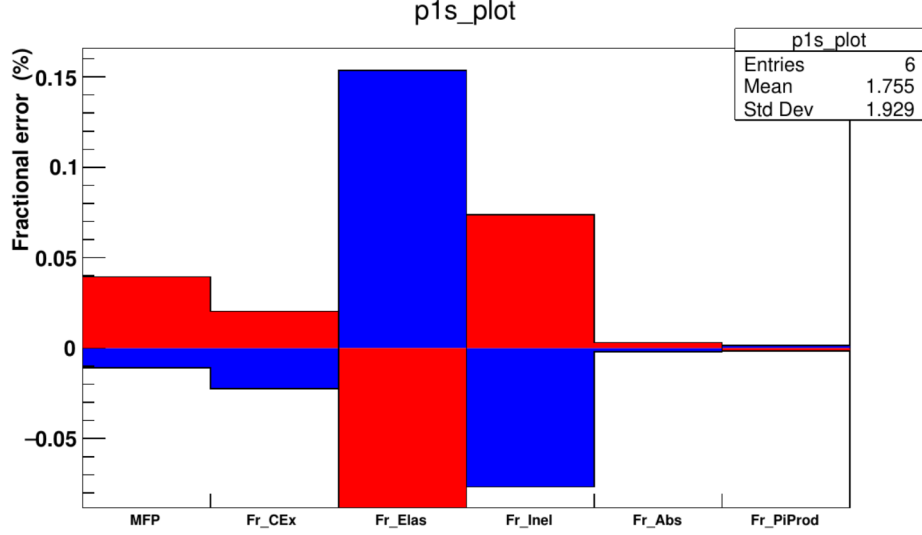
Figure 7.4: Tagging efficiency fractional uncertainties caused by the nucleon final state interaction model parameter variation for the FHC mode

Space (CHIPS) model for muon captures (based on non pertubative QCD) and two different routines for pion capture, one which is based on CHIPS and one based on intra-nuclear cascade.

Because any change in the model can alter the energy spectra of the neutrons, these alternative functions can be used to estimate the fractional uncertainties for the tagging efficiency. This is done by using the MC regeneration method, where the nominal Monte Carlo is regenerated by replacing the default Geant4 routines with the alternative ones in order to see the varaition in the tagging efficiency value. For the alterantive muon capture model and the two alternative pion capture models, the fractional discrepancies are shown in Equation 7.11.

$$\delta_{muonCHIPS} = \frac{T_{muonCHIPS} - T_{nom}}{T_{\text{nom}}}$$
$$\delta_{pionCHIPS} = \frac{T_{pionCHIPS} - T_{nom}}{T_{\text{nom}}} \qquad (7.11)$$
$$\delta_{pionBert} = \frac{T_{pionBert} - T_{nom}}{T_{\text{nom}}}$$

Chapter 8

Conclusion